Environmental Science & Technology

Article

pubs.acs.org/est

Iron(II)-Catalyzed Iron Atom Exchange and Mineralogical Changes in Iron-rich Organic Freshwater Flocs: An Iron Isotope Tracer Study

Laurel K. ThomasArrigo,[†] Christian Mikutta,*[,†] James Byrne,[‡] Andreas Kappler,[‡] and Ruben Kretzschmar[†]

[†]Soil Chemistry Group, Institute of Biogeochemistry and Pollutant Dynamics, Department of Environmental Systems Science, CHN, ETH Zurich, Universitätstrasse 16, CH-8092 Zurich, Switzerland

[‡]Geomicrobiology Group, Centre for Applied Geosciences (ZAG), University of Tübingen, Sigwartstrasse 10, D-72076, Tübingen, Germany

Supporting Information

ABSTRACT: In freshwater wetlands, organic flocs are often found enriched in trace metal(loid)s associated with poorly crystalline Fe(III)-(oxyhydr)oxides. Under reducing conditions, flocs may become exposed to aqueous Fe(II), triggering Fe(II)-catalyzed mineral transformations and trace metal(loid) release. In this study, pure ferrihydrite, a synthetic ferrihydrite-polygalacturonic acid coprecipitate (16.7 wt % C), and As-(1280 and 1230 mg/kg) and organic matter (OM)-rich (18.1 and 21.8 wt % C) freshwater flocs dominated by ferrihydrite and nanocrystalline lepidocrocite were reacted with an isotopically enriched ^{57}Fe(II) solution (0.1 or 1.0 mM Fe(II)) at pH 5.5 and 7. Using a combination of wet chemistry, Fe isotope analysis, X-ray absorption spectroscopy (XAS), ^{57}Fe Mössbauer spectroscopy and X-ray diffraction, we followed the Fe atom exchange kinetics and secondary mineral formation over 1 week. When reacted with Fe(II) at pH 7, pure ferrihydrite exhibited rapid Fe atom exchange at both Fe(II) concentrations, reaching 76 and 89% atom exchange in experiments with 0.1 and 1 mM Fe(II), respectively. XAS data revealed that it transformed into goethite (21%) at the lower Fe(II) concentration and into lepidocrocite (73%) and goethite (27%) at the higher Fe(II) concentration. Despite smaller Fe mineral particles in the coprecipitate and flocs as compared to pure ferrihydrite (inferred from Mössbauer-derived blocking temperatures), these samples showed reduced Fe atom exchange (9−30% at pH 7) and inhibited secondary mineral formation. No release of As was recorded for Fe(II)-reacted flocs. Our findings indicate that carbohydrate-rich OM in flocs stabilizes poorly crystalline Fe minerals against Fe(II)-catalyzed transformation by surface-site blockage and/or organic Fe(II) complexation. This hinders the extent of Fe atom exchange at mineral surfaces and secondary mineral formation, which may consequently impair Fe(II)-activated trace metal(loid) release. Thus, under short-term Fe(III)-reducing conditions facilitating the fast attainment of solid-solution equilibria (e.g., in stagnant waters), Fe-rich freshwater flocs are expected to remain an effective sink for trace elements.

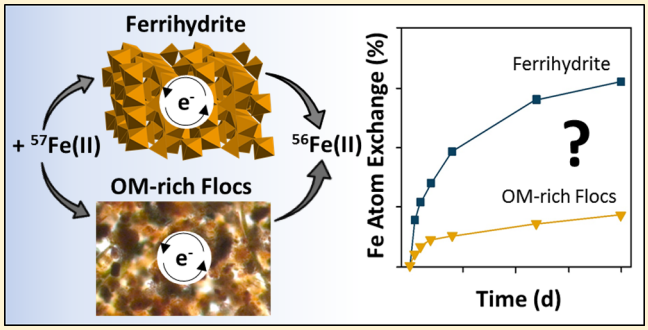

INTRODUCTION

Iron-rich organic flocs are often observed in freshwater wetlands and tend to show high affinities for trace metal(loid)s.[1−5] Iron mineral phases existing within flocs play a dominant role in trace metal(loid) sorption, with the highest trace metal(loid) concentrations associated with poorly crystalline Fe(III)-(oxyhydr)oxides,[1−5] and lower trace metal(loid) concentrations linked to more crystalline minerals and organic/sulfide-associated Fe(II).[4,5] Precipitation of Fe minerals in freshwater wetlands may occur through the (a)biotic oxidation of Fe(II), and can be influenced by the geochemical conditions such as pH, temperature, and the presence of (in)organic compounds in the surrounding water.[6−8] Pelagic freshwater flocs have been shown to create unique geochemical microenvironments which are independent of the surrounding surface water's geochemical conditions.[5,9−12] These microenvironments show steep pH and O_2 gradients facilitated by the consortial coexistence of Fe(III)-reducing (IRB) and Fe(II)-oxidizing (IOB) bacteria,[5,10,13,14] enabling aggregate microbial communities to thrive in surface water geochemical conditions previously considered inhospitable.[9,10] For example, Elliot et al.[10] recently identified collaborative IRB and IOB existing in freshwater flocs in Canadian lakes with O_2 concentrations ranging from micro-oxic to O_2-saturated. As a result of these microenvironments, Fe cycling within freshwater flocs is likely controlled by microbially produced Fe(II); influencing floc-Fe mineral precipitation and recrystallization processes.

Received: March 22, 2017
Revised: May 17, 2017
Accepted: May 18, 2017
Published: June 7, 2017

DOI: 10.1021/acs.est.7b01495
Environ. Sci. Technol. 2017, 51, 6897−6907

Adsorption of Fe(II) to Fe(III)-(oxyhydr)oxides has been shown to lead to the oxidation of surface-adsorbed Fe(II), the transfer of electrons to structural Fe(III), the release of structural Fe(III) as Fe(II) ("atom exchange"), and thus the recrystallization of the Fe(III)-(oxyhydr)oxide phase.[15−18] For crystalline Fe(III)-(oxyhydr)oxides like goethite (α-FeOOH) and hematite (α-Fe_2O_3), Fe atom exchange can occur without secondary mineral formation.[15,16,19] In contrast to these crystalline Fe(III)-(oxyhydr)oxides, ferrihydrite (e.g., ~$Fe_5HO_8{\cdot}4H_2O$) and nano-lepidocrocite (γ-FeOOH) contained in freshwater flocs[3,4] are comparably unstable, and their Fe(II)-catalyzed recrystallization into more stable Fe(III) mineral phases is well documented.[17,20−22] Depending on Fe(II) concentrations, pH, and background ligand, resulting secondary minerals can include lepidocrocite, goethite, and magnetite (Fe_3O_4).[17,20−22] Using ^{55}Fe-labeled Fe(III)-(oxyhydr)oxides, Pedersen et al.[21] found that the Fe(II)-catalyzed mineral transformations of ferrihydrite and lepidocrocite (5 nm-sized) proceeded equally fast (<3 days), whereas those of 20 nm-sized lepidocrocite and goethite required longer (>7 days); attributing this to an effect of particle size. In addition, mineral transformations may be hindered by the presence of surface-associated or structurally incorporated elements. While low concentrations of coprecipitated or adsorbed As (As:Fe mol ratio = <0.035) are not expected to impact ferrihydrite recrystallization and transformation rates,[23,24] high concentrations of As (As:Fe molar ratio ≥0.035) have been shown to inhibit ferrihydrite transformation into lepidocrocite,[24,25] and similar effects have been recorded for Al,[26] Mo,[25] and Si.[27] Similarly, Jones et al.[27] found that 25 or 150 mg/L of dissolved OM (Suwannee River fulvic acid) effectively hindered the Fe(II)-catalyzed transformation of ferrihydrite and lepidocrocite. Chen et al.[28] showed that ferrihydrite coprecipitated with different amounts of a carboxylic-rich OM extracted from fresh litter samples from the O horizon of an Ultisol (C:Fe molar ratio = 0−1.6) displayed a linear decrease in mineral transformation rates with increasing C concentrations.

Recrystallization or mineral transformation of Fe(III)-(oxyhydr)oxides may affect the solid-solution distribution of trace metal(loid)s. While dissimilatory Fe(III) reduction triggers the release of associated As,[29,30] the effect of Fe(II)-catalyzed mineral changes is not as clear. For example, in reacting arsenate-adsorbed ferrihydrite (As:Fe molar ratio = 0.224, 10 g/L) with 0.5 and 10.0 mM Fe(II) at circumneutral pH, Gomez et al.[25] recorded As releases of up to 0.42 mM, accounting for <1% of As_{total}. In similar experiments, Pedersen et al.[23] followed the Fe(II)-catalyzed reduction of arsenate-loaded ferrihydrite and lepidocrocite (As:Fe molar ratio = 0−0.005; 0.5 mM Fe(III)/L) in the presence of up to 1.0 mM Fe(II) at pH 6.5, reporting a decrease in surface-associated arsenate and an absence of aqueous As, which they interpreted as evidence for the structural incorporation of arsenate into secondary Fe(III) minerals. The Fe(II)-catalyzed structural incorporation of surface-adsorbed Cu, Ni, U, and/or Zn has also been evidenced for ferrihydrite and goethite,[31−34] whereas the Fe(II)-catalyzed release of preincorporated Co, Cu, Mn, Ni, and Zn has been reported for goethite.[31,35] This potential cycling of trace metal(loid)s through Fe(III)-(oxyhydr)oxides in the presence of Fe(II) may be of particular importance in dynamic environments like freshwater wetlands which frequently experience seasonal changes in redox potential.

In a previous study, we used ^{57}Fe Mössbauer spectroscopy and synchrotron X-ray techniques to characterize naturally occurring Fe-rich organic flocs from freshwater streambeds of the As-enriched peatland *Gola di Lago* (Switzerland), finding a carbohydrate-rich OM fraction (18−35 wt % C) and 34−2620 mg/kg As (arsenate and arsenite) bound in monodentate-binuclear ("bridging") surface complexes to ferrihydrite and disordered lepidocrocite.[3] *Gola di Lago* flocs tend to settle under low-flow stream conditions[3] and through either burial or seasonally induced shifts in the dominant microbial groups[5,10] may eventually be exposed to Fe(III)- or sulfate-reducing conditions. Recently, we showed that reaction of floc ferrihydrite and lepidocrocite with dissolved sulfide triggered the rapid (≤0.3 days) precipitation of mackinawite (FeS) and the release of up to 73% of mineral-associated As.[4] The fast rate of mineral-phase transformation was attributed to the small particle sizes of floc-Fe minerals,[3,4] likely resulting from the presence of OM during Fe(II) oxidation.[36] For this same reason, it seems likely that the rapid Fe(II)-catalyzed (re)crystallization of floc Fe minerals would similarly elicit the release of As.[25,29,30] Alternatively, the carbohydrate-dominated OM fraction in freshwater flocs may stabilize Fe minerals against Fe(II)-catalyzed (re)crystallization,[27,28,37] thereby hindering the release of floc-associated trace metal(loid)s, including As. To date, extensive research has been conducted on the Fe(II)-catalyzed transformation of synthetic Fe(III) minerals and coprecipitates.[17,20−22,27,28,37] However, neither the kinetics of Fe atom exchange nor the net effect of Fe(II) on freshwater floc mineralogy and their associated trace metal(loid)s is known; information which is critical to understanding the role of freshwater flocs in trace metal(loid) cycling under Fe(III)-reducing conditions. Therefore, we studied Fe(II)-catalyzed mineral transformations in natural As-enriched freshwater flocs and their effect on As release, and hypothesized that carbohydrate-rich OM in flocs stabilizes Fe(III)-(oxyhydr)oxides, slowing the Fe atom exchange kinetics and inhibiting secondary mineral formation. To better clarify the role of floc OM in Fe(II)-induced mineralogical changes this study additionally included a synthetic ferrihydrite and ferrihydrite-OM coprecipitate. We employed ^{57}Fe(II) as a stable isotope tracer in combination with X-ray absorption spectroscopy (XAS), ^{57}Fe Mössbauer spectroscopy, and X-ray diffraction to track Fe atom exchange, Fe(II)-catalyzed mineral-phase changes, and in case of As-rich freshwater flocs, their effect on trace metalloid release.

MATERIALS AND METHODS

Floc Sampling, Preparation, and Characterization. Floc material was collected from streambeds of the *Gola di Lago* peatland (Supporting Information (SI) Figure S1) in October 2013. Flocs were collected in open beakers, allowed to settle overnight, and were then decanted, transported to the laboratory, and stored at 4 °C in darkness until further processing. The flocs were wet-sieved into <40 μm and 40−250 μm size fractions, hereafter referred to as "5S" and "5L" (small and large flocs from site 5, respectively), as described in ref 4. Standard geochemical parameters (pH, E_h, T, dissolved O_2, and electrical conductivity) of the surrounding surface waters were determined at the time of floc collection and can be found in ref 4.

Ferrihydrite and Coprecipitate Synthesis. In this study, natural flocs were compared against a synthetic ferrihydrite and a ferrihydrite-polygalacturonic acid coprecipitate (Fh-PGA).

DOI: 10.1021/acs.est.7b01495
Environ. Sci. Technol. 2017, 51, 6897−6907

PGA was used as a proxy for the acid carbohydrate-rich OM fraction found in *Gola di Lago* freshwater flocs.[3] The synthesis of the ferrihydrite and Fh-PGA coprecipitate is described briefly: All solutions used were prepared from doubly deionized (DDI) water (Milli-Q, ≥ 18.2 MΩ·cm). Ferrihydrite was prepared by adding 1 M NaOH (Titrisol) to 500 mL of a solution containing 100 mmol of Fe(III) as $Fe(NO_3)_3{\cdot}9H_2O$ (Merck) under vigorous stirring (1200/min) until a pH of 7.0 ± 0.1 was obtained.[38] The Fh-PGA coprecipitate was synthesized following Mikutta et al.:[36] 1 g of PGA $(C_6H_8O_6)_n$, ≥ 90% (enzym.), Sigma-Aldrich) was equilibrated overnight in 1 L DDI water adjusted to pH 7.0 with 1 M NaOH in darkness and under vigorous stirring (1200/min). The PGA solution was then acidified to pH 4.0 with 1 M HNO_3 (Titrisol) and purged with $N_2(g)$ for 15 min. 50 mL of a solution containing 10 mmol of Fe(III) as $Fe(NO_3)_3{\cdot}9H_2O$ (Merck) were then added, followed by the addition of 1 M NaOH as described in the synthesis of ferrihydrite. The final C:Fe molar ratio of the coprecipitate was 2.5 ± 0.3 (n = 2), similar to C:Fe molar ratios we previously reported for flocs.[3,4] The ferrihydrite and Fh-PGA coprecipitate were then repeatedly centrifuged at 3500g for 15 min and resuspended in 700 mL DDI water until the electric conductivity of the supernatants was ≤100 μS/cm. Afterward, the suspensions were shock-frozen by dropwise injection into liquid N_2,[39] freeze-dried, manually homogenized with a mortar and pestle, and stored in brown glass bottles in a desiccator until use.

^{57}Fe(II) Isotope Tracer Experiment. ^{57}Fe(II) was used as a stable isotope tracer to explore Fe(II)-catalyzed mineral transformations and Fe atom exchange kinetics in freshwater flocs and synthetic (co)precipitates. The entire experiment was conducted in triplicates in a glovebox (N_2 atmosphere, < 10 ppm (v/v) O_2). Dried sample material (500 mg) was placed in serum bottles and equilibrated for 16 h in 250 mL of anoxic 50 mM 3-(*N*-morpholino)propanesulfonic acid (MOPS) or 2-(N-morpholino)ethanesulfonic acid (MES) buffer adjusted to pH 7 (MOPS) or pH 5.5 (MES). Solid-phase Fe concentrations ranged from 628 to 1104 mg/L (SI Table S1). A ^{57}Fe-enriched stock solution of 100 mM Fe(II) was prepared by dissolving ^{57}Fe metal powder (95.06% ^{57}Fe, Isoflex, San Francisco, CA) in 2 M HCl at 70 °C overnight, which was then purged with $N_2(g)$, sealed, and transferred into the glovebox. The Fe concentration of the ^{57}Fe(II) solution was determined in 0.22 μm filtrates with inductively coupled plasma-optical emission spectrometry (ICP-OES, Agilent 5100). Reactions were started when 0.22 μm filtered aliquots of the ^{57}Fe(II) stock solution were added to the serum bottles (0.1 or 1.0 mM Fe(II), SI Table S1), which were then capped with butyl rubber stoppers. All treatments remained under the mmol Fe(II)/g ferrihydrite ratio of unity at which magnetite precipitation is expected.[20] The serum bottles were wrapped in Al foil and horizontally shaken (150 rpm) at 25 ± 1 °C for 1 week. Following initial pH adjustments in the first 15 min, the pH remained at 7.0 ± 0.1 or 5.5 ± 0.1 throughout the experiment. Iron(II)-free controls were included for each treatment to quantify aqueous As and Fe releases originating from solid-phase dissolution.

Total Aqueous Concentrations and Element Contents. Aliquots for aqueous-phase analysis (10 mL) were taken at 0, 3, 6, 12, 24, 72, 120, and 168 h. Total aqueous element concentrations, including As, were determined in 0.22-μm nylon filtrates with inductively coupled plasma-mass spectrometry (ICP-MS, Agilent 8800 Triple Quad) or ICP-OES. Additional aqueous samples were taken at selected time points (0, 24, and 168 h) and filtered through 0.025-μm cellulose filters to test for contributions of particulate Fe (>0.025 μm) in the 0.22 μm filtrates using ICP-OES.

Material for solid-phase analysis was collected on 0.45-μm cellulose filters and thoroughly rinsed with anoxic DDI water. The filter residues were covered and dried in the glovebox atmosphere. Triplicate samples were combined, homogenized with a mortar and pestle, and stored in darkness until further analyses. (Un)reacted flocs and the Fh-PGA coprecipitate were dissolved using microwave-assisted acid digestion (MLS turboWAVE) while (un)reacted ferrihydrite was dissolved in 67% HNO_3 at 60 °C (n = 2). Total element contents in the digests were determined using ICP-OES, and total C contents of (un)reacted flocs and the Fh-PGA coprecipitate were analyzed with an elemental analyzer (CHNS-932, LECO; n = 2).

Estimation of Iron Atom Exchange. Aqueous and solid-phase Fe isotope compositions were determined with ICP-MS. Samples for isotope analysis were diluted to ∼30 μg/L Fe and measured in reaction cell mode with a H_2 gas flow rate of 7 mL/min to remove argide polyatomic interferences. The accuracy of this method was tested with the Fe isotopic reference material IRMM-014.[40] Further details regarding method validation can be found in the SI. Interferences from ^{58}Ni were accounted for through monitoring ^{60}Ni counts, though were found to be negligible. Iron isotope mole fractions (f) were calculated by dividing the counts per second (cps) of the Fe isotope n by the sum of the total Fe isotope's cps:

$$\frac{{}^{n}\mathrm{cps}}{{}^{54}\mathrm{cps} + {}^{56}\mathrm{cps} + {}^{57}\mathrm{cps} + {}^{58}\mathrm{cps}} \times 100 = f^{n}\mathrm{Fe}(\%) \quad (1)$$

The use of stable Fe isotopes enables the investigation of atom exchange between Fe(III) minerals and aqueous Fe (Fe_{aq}). In this study, a highly enriched ^{57}Fe(II) solution (f^{54}Fe: 0.04%, f^{56}Fe: 3.04%, f^{57}Fe: 95.06%, f^{58}Fe: 1.86%) was reacted with materials containing Fe(III)-(oxyhydr)oxides of near natural Fe isotope abundance (f^{54}Fe: ∼4.88%, f^{56}Fe: ∼92.73%, f^{57}Fe: ∼2.09%, f^{58}Fe: ∼0.31%, SI Tables S5−7). Because adsorption or desorption reactions alone would not significantly alter the isotopic composition of the aqueous-phase Fe, deviations from the initial isotopic composition of Fe_{aq} would therefore indicate Fe atom exchange between the aqueous and solid phase. In order to maintain environmentally relevant Fe(II) concentrations,[3,4,41,42] the Fe(II) concentrations used in this study were comparatively low. Therefore, the $Fe(II)_{spike}$:Fe_{solid} ratio used here was small (0.005−0.072 mol/mol, SI Table S1). Because of this, the Fe isotope composition of the solid-phase is expected to change more slowly than that of Fe_{aq} because Fe atoms must cycle through multiple times before complete Fe atom exchange occurs in the solid-phase.[16] Theoretically, an identical isotopic composition in both aqueous and solid-phase Fe would indicate the system reached isotopic equilibrium. In this experiment, the solid-phase Fe isotope composition was determined at days 0 and 7 for comparison.

A standard approach to interpret isotope data, which accounts for differences in pool sizes in aqueous and solid-phase Fe, is the calculation of the percent of Fe atoms exchanged:[16,19]

DOI: 10.1021/acs.est.7b01495
Environ. Sci. Technol. 2017, 51, 6897−6907

$$\frac{N_{\mathrm{Fe(II)}}(f^n\mathrm{Fe(II)}_i - f^n\mathrm{Fe(II)}_t)}{N_{\mathrm{solid}}(f^n\mathrm{Fe(II)}_t - f^n\mathrm{solid}_i)} \times 100 = \mathrm{Fe\ atoms\ exchanged(\%)} \quad (2)$$

where $N_{\mathrm{Fe(II)}}$ is the number of moles of Fe(II) added to solution and N_{solid} the moles of Fe in the initial solid-phase. $f^n\mathrm{Fe(II)}_i$ and $f^n\mathrm{solid}_i$ are the initial fractions of Fe isotope n in the $\mathrm{Fe_{aq}}$ and solid-phase Fe, respectively, and $f^n\mathrm{Fe(II)}_t$ is the fraction of Fe isotope n in the $\mathrm{Fe_{aq}}$ at time t. Because of the poorly crystalline nature of the samples' Fe minerals and their propensity to dissolve (Figure 1),[3,4,43] sequential extractions to distinguish between "adsorbed" and "incorporated" Fe(II) were not possible. Therefore, we used changes in the $\mathrm{Fe_{aq}}$ isotope composition to calculate the extent of Fe atom exchange. Though this could lead to an overestimation of atom exchange by excluding potentially adsorbed Fe(II), recent studies suggest that electron transfer between adsorbed Fe(II) and the solid-phase occurs quickly and that surface-associated Fe(III) may be rapidly incorporated into the solid-phase during the initial Fe(II) adsorption.[17,44] No correction for mass-dependent isotope fractionation was included as fractionation between Fe(II) and ferrihydrite results in changes of only a few per mil ($^{56/54}$Fe equilibrium fractionation factor ~ −3.2‰);[45] insignificant compared to the effect induced by the ^{57}Fe(II) enriched solution used in this study ($\delta^{57/56}$Fe = +1,352,300‰).

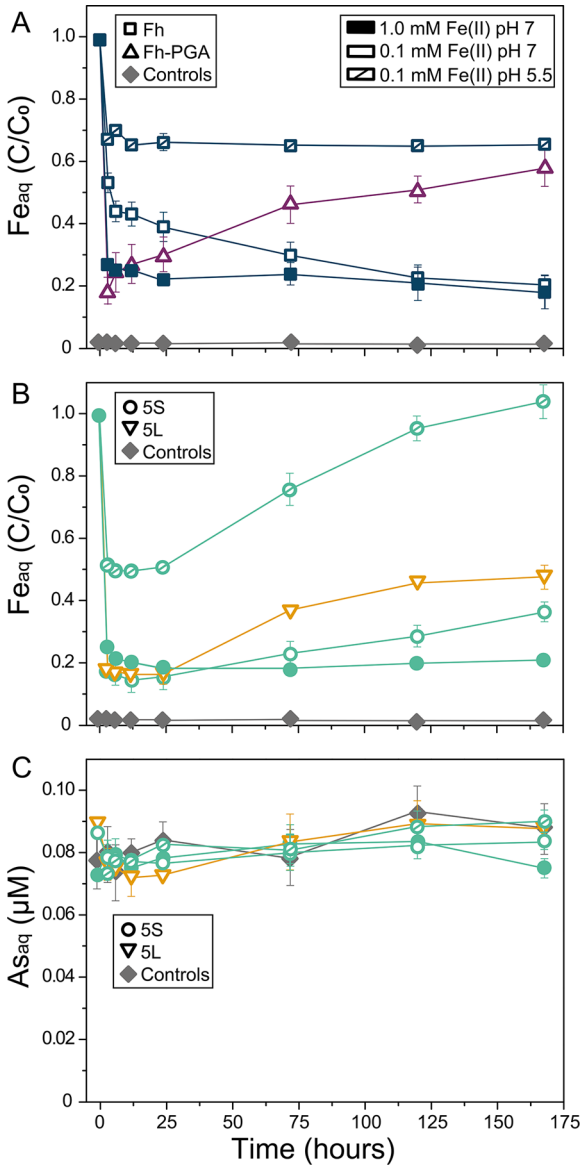

Figure 1. Trends in dissolved Fe (A and B) and As (C) determined in 0.22 μm filtrates. Error bars representing the standard deviation from triplicate experiments are either shown or are smaller than the symbol size. Fe(II)-free controls were included for each sample shown. In all controls, $\mathrm{Fe_{aq}}$ concentrations remained <0.01 mM, and $\mathrm{As_{aq}}$ ranged between 0.06 and 0.10 μM for the duration of the experiment. Dissolved Fe concentrations are shown normalized to the initial concentration of the Fe(II) spike.

X-ray Diffraction. Qualitative mineral-phase analyses were performed by powder X-ray diffraction (XRD, D8 Advance, Bruker), for which homogenized samples were loaded into 1 mm o.d. borosilicate glass capillaries and analyzed in Bragg–Brentano geometry using Cu Kα radiation (λ = 1.5418 Å, 40 kV and 40 mA) and a high-resolution energy-dispersive 1-D detector (LYNXEYE). Fe(II)-reacted samples were prepared for XRD measurements under anoxic conditions. Diffractograms were recorded from 10 to 80°2θ with a step size of 0.02°2θ and 10 s acquisition time per step. Experimental data were corrected by subtracting the diffractogram of an empty capillary. Further background subtraction was conducted in DIFFRAC.EVA (Bruker).

Iron X-ray Absorption Spectroscopy. To determine speciation changes of solid-phase Fe after ^{57}Fe(II)-catalyzed mineral-phase transformation, (un)reacted samples were analyzed by Fe K-edge (7112 eV) XAS at beamline 13 ID-E of the Advanced Photon Source (APS, Chicago, IL). For these analyses, samples were pressed into 1.3 cm pellets and sealed with Kapton tape. Fe(II)-reacted samples were prepared under anoxic conditions and kept anoxic until the end of the XAS measurements. Iron K-edge X-ray absorption near edge structure (XANES) and extended X-ray absorption fine structure (EXAFS) spectra were recorded in transmission mode at ~40 K using a He(l) cryostat. The Si(111) monochromator was calibrated to the first-derivative maximum of the K-edge absorption spectrum of a metallic Fe foil (7112 eV). The foil was continuously monitored to account for small energy shifts (<1 eV) during the sample measurements. Higher harmonics in the beam were eliminated by detuning the monochromator by 40% of its maximal intensity. Three to seven scans per sample were collected and averaged. All spectra were energy calibrated, pre-edge subtracted, and postedge normalized in Athena[46] with the edge energy, E_0, defined as the zero-crossing in the second XANES derivative. Linear combination fit (LCF) analyses of k^3-weighted EXAFS spectra were performed in Athena[46] over a k-range of 2–10 Å^{-1} with the E_0 of all spectra and reference compounds set to 7128 eV. No constraints were imposed on the fits, and initial fit fractions (100 ± 12%) were recalculated to a component sum of 100%. Initial inclusion of organically complexed Fe(II/III) reference compounds proved nonviable; therefore, final fits were conducted with ferrihydrite, goethite, and lepidocrocite as fit references.

^{57}Iron Mössbauer Spectroscopy. Mössbauer spectra of selected samples were obtained with a ^{57}Co/Rh γ-radiation source with an activity of ~35 mCi vibrated in constant acceleration mode in a standard setup (WissEl, Wissenschaftliche Elektronik GmbH). Anoxic sample material (30–60 mg) was loaded into Plexiglas sample holders (~1 cm^2) in a glovebox (100% N_2; MBraun) under anoxic conditions, while

DOI: 10.1021/acs.est.7b01495
Environ. Sci. Technol. 2017, 51, 6897–6907

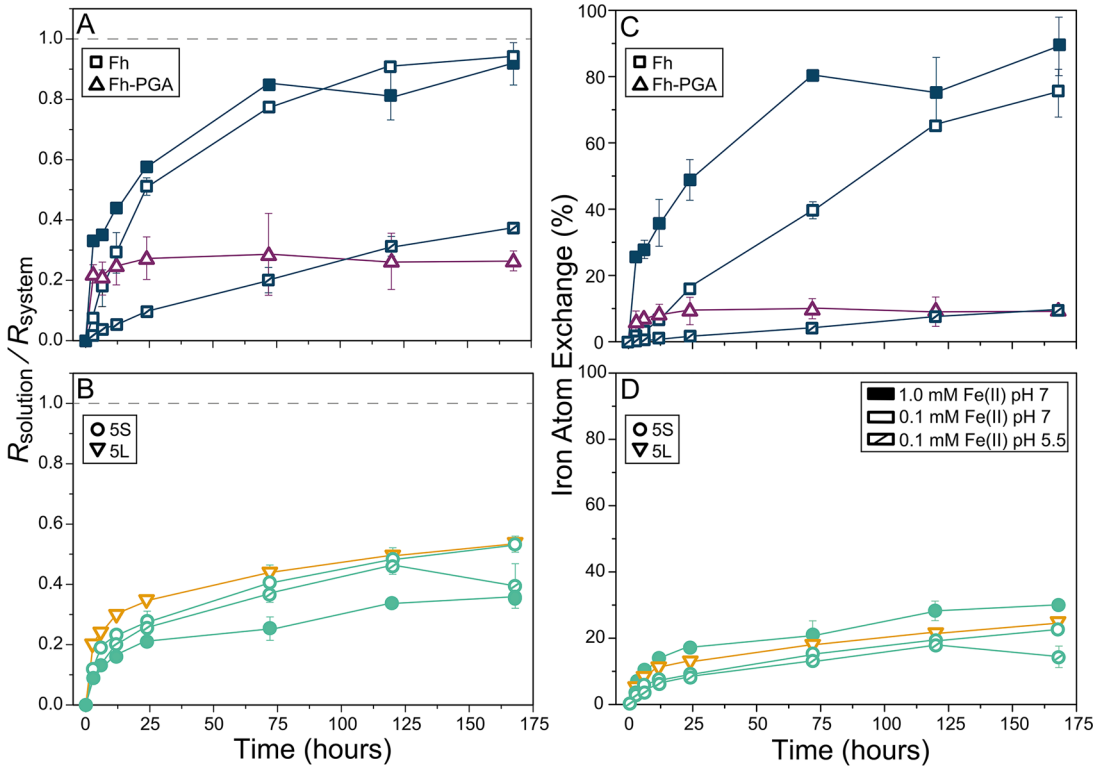

Figure 2. (A, B) Changes in $R_{solution}$ normalized to R_{system}. Here, $R_{solution}$ and R_{system} refer to the $f^{56}Fe$:$f^{57}Fe$ ratio of the solution and the system, respectively. (C, D) Percent of Fe atoms exchanged as calculated from eq 2. Error bars representing the standard deviation from triplicate experiments are either shown or are smaller than the symbol size. Standard deviations of $R_{solution}/R_{system}$ were derived using error propagation.

oxic samples were prepared in air. All samples were mounted in transmission geometry. Sample temperatures were varied with a closed-cycle cryostat (SHI-850-I, Janis Research Co.), whereas the ^{57}Co/Rh source remained at room temperature. Spectra were collected between 77 and 5 K, and were analyzed using the Recoil software (University of Ottawa, Canada) by applying an extended Voigt-based fitting routine.[47] The spectra were calibrated against 7 μm thick α-$^{57}Fe^0$ at 295 K and center shifts (*CS*) are quoted relative to this. For all samples the half width at half-maximum was fixed to 0.13 mm/s; the value of the inner line broadening of the calibration foil at 295 K. Because all samples initially contained natural-abundance Fe ($f^{57}Fe \sim 2.12\%$), the ^{57}Fe spikes resulted in $^{57}Fe(II)_{spike}$:$^{57}Fe_{native}$ ratios of 0.23−3.28 (SI Table S1), thus Mössbauer spectra of reacted samples also contains information from native Fe atoms.

RESULTS AND DISCUSSION

Dissolved Fe and As. Figure 1 shows the temporal evolution in dissolved Fe (C/C_0) and As over the duration of the experiment. Absolute Fe_{aq} concentrations are shown in SI Figure S2. The immediate decrease in Fe_{aq} can be attributed to the initial adsorption of Fe(II) onto Fe(III)-(oxyhydr)-oxides,[17,21,48] which proceeded similarly among samples in comparable treatments. Differences in initial Fe adsorption are largely ascribed to pH, with pH 7 treatments showing larger decreases in Fe_{aq} (48−84%, $\bar{x}$ = 74%) within the first 3 h compared to decreases of only 34 and 50% for pure ferrihydrite and floc sample 5S at pH 5.5 (Figure 1). This is consistent with decreased Fe(III)-(oxyhydr)oxide reactivity toward Fe(II) adsorption at lower pH.[16] Following this initial net mass transfer, Fe_{aq} remained mostly stable in treatments through the first 24 h (Figure 1). Thereafter, Fe_{aq} in the ferrihydrite series remained relatively unchanged for the duration of the experiment, whereas flocs and the Fh-PGA coprecipitate showed increases in Fe_{aq} starting after 24 h. This may be caused by mineral transformations into more crystalline Fe minerals which results in the desorption of Fe(II),[49] through Fe(II)-induced particle dispersion or ligand-promoted Fe mineral dissolution.[43] Because the MOPS and MES buffers would mask slight changes in dissolved organic C concentrations, it was not possible to determine whether the increases in Fe_{aq} could be attributed to Fe-OM colloids,[28] though the stable C content in samples before and after reaction indicates no significant loss of solid-phase OM (SI Table S2). Dissolved Fe concentrations in Fe(II)-free controls were small (<0.01 mM), suggesting floc and Fh-PGA dissolution resulted primarily from spiked Fe(II) and that microbial Fe(III) reduction and electron transfer from the carbohydrate-rich OM to structural Fe(III) was negligible.

Changes in aqueous As concentrations in floc treatments were minimal (Figure 1) and did not exceed As concentrations measured in the Fe(II)-free controls (<0.1 μM). However, trends in As release after 24 h closely resembled those of Fe_{aq}, indicating that As release from flocs occurred primarily as a result of Fe(III)-(oxyhydr)oxide dissolution. This is further supported by similar Fe and As recoveries obtained in floc treatments (80−90% ($\bar{x}$ = 84%) and 80−89% ($\bar{x}$ = 85%), respectively). Though the majority of As remained solid-phase associated (Figure 1 and SI Table S2), rapid de- and re(ad)sorption cannot be excluded. The lack of significant As release is in agreement with similar studies on the Fe(II)-catalyzed reduction of ferrihydrite or goethite with surface-adsorbed Cu, Ni, U, and/or Zn,[31−34] and may indicate the structural incorporation of As into secondary Fe(III)

DOI: 10.1021/acs.est.7b01495
Environ. Sci. Technol. 2017, 51, 6897−6907

minerals.[23] Alternatively, it may imply only minor Fe(II)-induced mineral transformations in the flocs.

Iron Atom Exchange. Figures 2A and B illustrate that all treatments showed changes in Fe_{aq} isotopic composition over the duration of the experiment. This data is further summarized in SI Figure S3 and Tables S4−6. An isotope mass balance is presented in SI Table S7. The initial net mass transfer of Fe through $^{57}Fe(II)$ adsorption (Figure 1) alone does not alter the Fe_{aq} isotopic composition. Because initially ^{56}Fe is almost exclusively present in the solid-phase, increases in $f^{56}Fe$ of Fe_{aq} (SI Figure S3) indicate that solid-phase Fe atoms were simultaneously released; direct evidence of Fe atom exchange. All treatments showed significant changes in the $R_{solution}/R_{system}$ ratio during the first 24 h (+0.32 ± 0.16, $\bar{x} \pm \sigma$, Figures 2A and B). Here, $R_{solution}$ and R_{system} refer to the $f^{56}Fe$:$f^{57}Fe$ ratio of the solution and system, respectively. Thereafter, a distinction could be made between reactions involving the pure ferrihydrite, where the isotopic composition of Fe_{aq} continued steadily toward system equilibrium (+0.35 ± 0.08 after 24 h), and reactions involving the Fh-PGA and floc samples, where further changes in the $R_{solution}/R_{system}$ ratios were minimal (+0.15 ± 0.10). Accordingly, after 7 days, the isotopic composition of Fe_{aq} in pure ferrihydrite treatments reacted at pH 7 nearly reached system equilibrium, whereas Fh-PGA and floc samples hovered at or below 50% of the expected equilibrium composition (Figures 2A and B).

The percent of Fe atom exchange, calculated from eq 2, is presented in Figures 2C and D. The highest values were obtained for pure ferrihydrite reacted at pH 7 (75.7 and 89.0% for 0.1 and 1.0 mM Fe(II), respectively; Figure 2C, SI Tables S4 and S6). Reacting ferrihydrite at pH 5.5 resulted in significantly less Fe atom exchange (10.0%, Figure 2C, SI Table S5). In contrast to ferrihydrite, the Fh-PGA coprecipitate reacted at pH 7 resulted in the lowest Fe atom exchange recorded (9.2%, Figure 2C, SI Table S4), despite a similar initial Fe(II) adsorption (Figure 1) and a larger $^{57}Fe(II)_{spike}$:$^{57}Fe_{native}$ ratio (0.40 versus 0.23, SI Table S1). Likewise, floc samples, with $^{57}Fe(II)_{spike}$:$^{57}Fe_{native}$ ratios of 0.33−3.28, showed a similarly reduced Fe atom exchange when reacted at pH 7 (21.9−29.7%, $\bar{x}$ = 25.4%, Figure 2D). Similar to the ferrihydrite, floc sample 5S reacted at pH 5.5 achieved only 13.9% Fe atom exchange (Figure 2D, SI Table S5). The consistently lower extent of Fe atom exchange at lower pH agrees with the current consensus that adsorption of Fe(II) precedes Fe atom exchange,[15−17] with less Fe(II) adsorption at lower pH (Figure 1).[16,50]

Solid-Phase Mineral Transformations. X-ray diffraction patterns of (un)reacted samples are displayed in SI Figure S4. Ferrihydrite initially featured two broad peaks at 2.54 and 1.49 Å. When reacted with Fe(II) at pH 7, defined peaks attributed to crystalline goethite and lepidocrocite became apparent, with the prevalence of lepidocrocite at the higher initial Fe(II) concentration. In contrast, the diffractogram of ferrihydrite reacted at pH 5.5 did not indicate mineralogical changes; consistent with lower Fe(II) adsorption at lower pH (Figure 1). The XRD pattern of the initial Fh-PGA coprecipitate also displayed features of 2-line ferrihydrite;[36,38] however, unlike pure ferrihydrite, showed no crystalline-phase formation when reacted at pH 7. Initial XRD patterns for flocs showed diffuse scatter peaks with maxima corresponding to ferrihydrite and traces of quartz.[3,4] The broad peak at ∼3.2 Å may indicate a contribution from lepidocrocite, however, the absence of the dominant 020 lepidocrocite reflection at ∼6.26 Å implies an extremely small mean crystallite dimension perpendicular to 0k0.[6] After reaction with $^{57}Fe(II)$ at circumneutral pH, neither of the floc samples showed visible changes in their XRD patterns except for slight variations in peak intensities (SI Figure S4).

In addition to XRD we used XAS and Mössbauer spectroscopy to identify and quantify Fe species present in the solid-phase before and after reacting the solids with Fe(II). Normalized Fe K-edge XANES spectra of all samples displayed a first-derivative maximum at ∼7128 eV, consistent with Fe(III) reference spectra (SI Figure S5). As expected from the low $Fe(II)_{spike}$:Fe_{solid} ratios (SI Table S1), no change was visible in the XANES spectra of reacted samples. Linear combination fits of k^3-weighted Fe K-edge EXAFS spectra are illustrated in SI Figure S6, and their results are summarized in Table 1. At

Table 1. Linear Combination Fit Results for Fe K-edge EXAFS Spectra of Samples Prior to ("Initial") and After Reaction with Fe(II) (Figure S6)[a]

sample	treatment	Fe	Fh	Gt	Lp	NSSR[b]	red. χ^2[c]
		(g/kg)		(%)			−
5S	initial	386	48		52	1.7	0.12
	0.1 mM Fe(II) pH 5.5	308	48		52	2.8	0.22
	0.1 mM Fe(II) pH 7	317	50		50	2.9	0.24
	1.0 mM Fe(II) pH 7	334	34	10	56	5.6	0.47
5L	initial	315	57		43	1.3	0.11
	0.1 mM Fe(II) pH 7	285	46		54	1.2	0.11
Fh	initial	552	100			1.6	0.08
	0.1 mM Fe(II) pH 5.5	581	100			3.3	0.16
	0.1 mM Fe(II) pH 7[d]	581	79	21		1.6	0.10
	1.0 mM Fe(II) pH 7	520		27	73	12.7	2.09
Fh-PGA	initial	315	100			2.1	0.13
	0.1 mM Fe(II) pH 7	339	100			5.3	0.28

[a]Abbreviations: Fh = ferrihydrite, Gt = goethite, Lp = lepidocrocite, PGA = polygalacturonic acid. [b]NSSR: Normalized sum of squared residuals ($100 \times \sum_i(data_i\text{-}fit_i)^2/\sum_i data^2$). [c]Fit accuracy (reduced χ^2 = $(N_{idp}/N_{pts})\sum_i((data_i\text{-}fit_i)/\varepsilon_i)^2(N_{idp}\text{-}N_{var.})^{-1}$. N_{idp}, N_{pts} and $N_{var.}$ are, respectively, the number of independent points in the model fit (18), the total number of data points (161), and the number of fit variables (1−3). ε_i is the uncertainty of the i^{th} data point.[64] [d]This sample may contain up to 10% lepidocrocite-Fe; however inclusion of the Lp reference resulted in a higher NSSR and red. χ^2.

neutral pH, pure ferrihydrite reacted with 1.0 mM Fe(II) transformed completely into lepidocrocite (73%) and goethite (27%). The presence of lepidocrocite was also noticeable in Fourier-transformed EXAFS spectra by the large second peak at ∼3.06 Å ($R + \Delta R$) originating mainly from edge-sharing Fe octahedra in the structure of lepidocrocite (SI Figure S6). For pure ferrihydrite reacted with 0.1 mM Fe(II) at pH 7, only goethite (21%) was detected with XAS as mineral transformation product, despite XRD evidence for lepidocrocite (SI Figure S4). This result may imply that the lepidocrocite fraction in this sample was smaller than the XAS detection limit of approximately 5−10 atom %. The complete transformation of

DOI: 10.1021/acs.est.7b01495
Environ. Sci. Technol. 2017, 51, 6897−6907

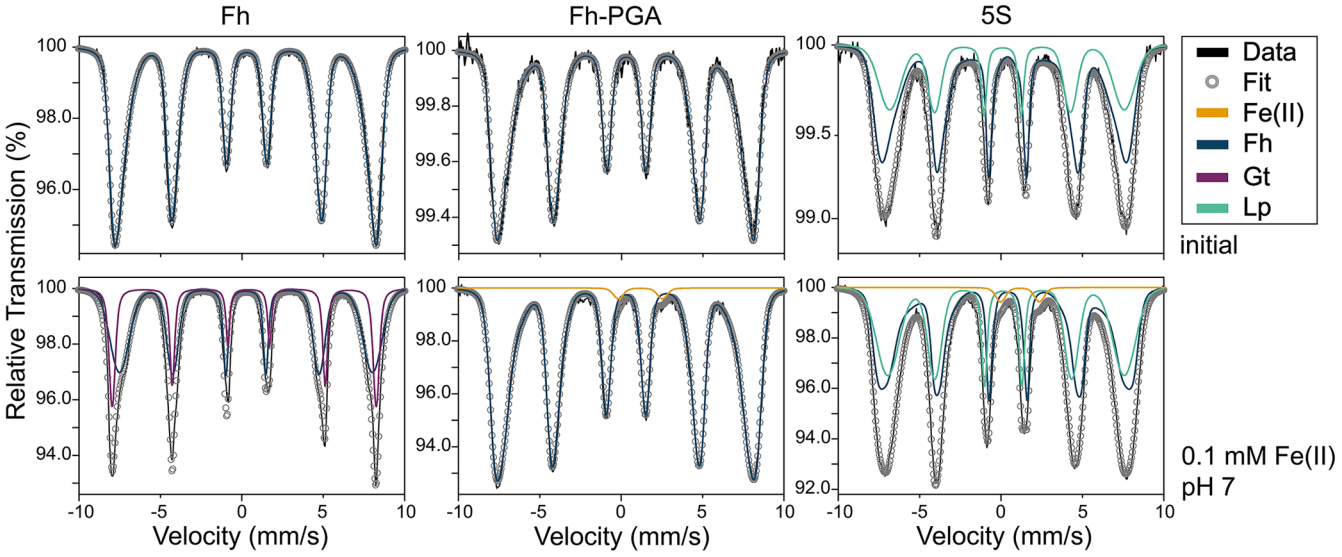

Figure 3. Mössbauer spectra of selected samples recorded at 5 K prior to ("initial") and after reaction with 0.1 mM Fe(II) at pH 7. In all graphs, black lines denote experimental data and circles represent the model fit. Additional spectra are presented in SI Figure S7, and the corresponding fit parameters are summarized in Table 2. Abbreviations: Fe(II) = adsorbed Fe(II), Fh = ferrihydrite, Gt = goethite, Lp = lepidocrocite.

Table 2. Mössbauer Parameters of Samples Measured at 5 K Prior to ("Initial") and After Reaction With Fe(II)

sample	treatment	species	CS[a] (mm/s)	ΔE_Q[b] (mm/s)	ϵ[c] (mm/s)	<|H|>[d] (T)	population[e] (%)
5S	initial	Fe(III)-S2	0.43		0.14	44.7	33.0 ± 2.9
		Fe(III)-S1	0.50		−0.10	42.5	67.0 ± 2.9
	0.1 mM Fe(II) pH 5.5	Fe(III)-S2	0.44		0.13	45.2	38.0 ± 1.4
		Fe(III)-S1	0.49		−0.12	42.0	61.5 ± 1.4
		Fe(II)-D	1.20	2.60			0.5 ± 0.2
	0.1 mM Fe(II) pH 7	Fe(III)-S2	0.40		0.09	45.0	45.0 ± 1.0
		Fe(III)-S1	0.54		−0.08	44.7	53.2 ± 1.0
		Fe(II)-D	1.35	2.38			1.8 ± 0.1
	1.0 mM Fe(II) pH 7	Fe(III)-S2	0.39		0.07	46.1	39.3 ± 0.6
		Fe(III)-S1	0.55		−0.08	41.1	59.1 ± 0.6
		Fe(II)-D	1.25	2.58			1.5 ± 0.2
5L	initial	Fe(III)-S2	0.46		0.12	44.5	44.1 ± 2.3
		Fe(III)-S1	0.49		−0.14	42.2	55.9 ± 2.3
	0.1 mM Fe(II) pH 7	Fe(III)-S2	0.44		0.14	45.2	37.5 ± 2.5
		Fe(III)-S1	0.48		−0.12	42.7	61.1 ± 2.5
		Fe(II)-D	1.15	2.37			1.3 ± 0.5
Fh	initial	Fh	0.46		−0.03	48.4	100.0
	0.1 mM Fe(II) pH 5.5	Fh	0.45		−0.02	48.3	100.0
	0.1 mM Fe(II) pH 7	Gt	0.48		−0.14	50.3	35.1 ± 0.5
		Fh	0.45		0.00	48.2	64.9 ± 0.5
	1.0 mM Fe(II) pH 7	Lp	0.51		0.01	46.3	71.3 ± 0.2
		Gt	0.47		−0.15	50.5	28.7 ± 0.2
Fh-PGA	initial	Fh	0.46		−0.03	46.8	100.0
	0.1 mM Fe(II) pH 7	Fh	0.47		0.00	47.1	98.4 ± 0.2
		Fe(II)-D	1.36	2.70			1.6 ± 0.2

[a]Center shift with respect to α-$^{57}Fe^0$. [b]Quadrupole splitting. [c]Quadrupole shift ($\epsilon = \Delta E_Q/2$). [d]Mean hyperfine field. [e]Spectral contribution and corresponding fit error. Abbreviations: Fh = ferrihydrite, Gt = goethite, Lp = lepidocrocite, PGA = polygalacturonic acid. Species assignments (S = sextet, D = doublet): Fe(III)-S1 = Fh, Fe(III)-S2 = Lp, Fe(II)-D = adsorbed Fe(II).

ferrihydrite seen at the higher Fe(II) concentration at pH 7 agrees with the high percentage of Fe atom exchange, and suggests that ferrihydrite largely recrystallized at the lower Fe(II) concentration (SI Figures S4 and S6; Table 1). At pH 5.5 ferrihydrite did not transform into crystalline Fe(III)-oxyhydroxides, consistent with the low percentage of Fe atom exchange observed. The same result was obtained for the Fh-PGA coprecipitate reacted with 0.1 mM Fe(II) at pH 7.

Unreacted floc samples 5S and 5L initially contained ferrihydrite (48 and 57%, respectively) and lepidocrocite; results which are in agreement with previous floc studies.[3,4] After reaction with Fe(II) at pH 7, the ferrihydrite fraction in flocs decreased by up to 14% ($\bar{x}$ = 7.6%), while concomitant increases were recorded for lepidocrocite (up to 11%, $\bar{x}$ = 4.3%) and goethite (10% with 1.0 mM Fe(II)). These small changes in floc mineralogy evidenced by XAS are consistent with the

DOI: 10.1021/acs.est.7b01495
Environ. Sci. Technol. 2017, 51, 6897−6907

nearly unaltered X-ray diffractograms of these samples (SI Figure S4). For both the Fh-PGA coprecipitate and floc samples, the minimal or lacking changes in solid-phase Fe speciation observed at pH 7 and 5.5 agree with the low extent of Fe atom exchange (Figure 2, SI Figures S4 and S6; Table 1). No changes in Fe mineral phases were observed for flocs reacted at pH 5.5.

Mössbauer spectra of samples collected at 5 K are displayed in Figure 3 and SI Figure S7, and fit parameters are reported in Table 2. The fits of the unreacted ferrihydrite and Fh-PGA coprecipitate spectra required only one sextet with parameters typical of ferrihydrite. However, the narrower mean hyperfine field (<|H|>) of the Fh-PGA coprecipitate (46.8 versus 48.4 T) likely indicates the influence of OM, which interferes with crystal growth, leading to smaller ferrihydrite crystals and more distorted Fe octahedra[28,51,52] (Table 2). In near perfect agreement with EXAFS LCF results (Table 1), the Mössbauer spectra revealed that ferrihydrite reacted with 1 mM Fe(II) at pH 7 transformed into lepidocrocite (71%) and goethite (29%), while at the lower Fe(II) concentration only goethite (35%) was determined as a mineral-transformation product (Table 2). Consistent with EXAFS results neither ferrihydrite reacted at pH 5.5 nor the Fh-PGA coprecipitate reacted at pH 7 showed evidence of secondary mineral formation.

Mössbauer spectra of floc samples 5S and 5L also confirmed our EXAFS results (Tables 1 and 2); unreacted floc samples showed Fe mineral compositions similar to those of previously studied flocs,[3] requiring two sextets (labeled Fe(III)-S1 and Fe(III)-S2) with < |H|> and quadrupole shifts (ϵ) indicative of disordered ferrihydrite[28,51,52] (Fe(III)-S1, <|H|> = 42.4 ± 0.2 T, ϵ = −0.12 ± 0.03 mm/s) and lepidocrocite[7,53] (Fe(III)-S2, <|H|> = 44.6 ± 0.1 T, ϵ = 0.13 ± 0.01 mm/s). Following reaction with Fe(II) at both pH 7 and 5.5, minor decreases in the ferrihydrite fraction (−9 ± 4%, $\bar{x} \pm \sigma$) were offset by increases in the lepidocrocite fraction (+8 ± 4%, $\bar{x} \pm \sigma$, Table 2). However, all Fe(II)-reacted floc and Fh-PGA samples required an additional Fe(II) doublet which contributed <2% to the total solid-phase Fe (Table 2). The center shift (CS) and ϵ determined for this Fe(II) species do not match typical values for Fe(II) adsorbed to mineral surfaces,[48] nor do its parameters match those of commonly measured Fe(II) minerals like siderite ($FeCO_3$)[54] or green rust ($[Fe(II)_{(1-n)}Fe(III)_n(OH)_2]^{n+}(CO_3,Cl,SO_4)^{n-}$).[55] Moreover, because the Fe(II) doublet was absent in all ferrihydrite samples, it is plausible that this spectral feature represents organically complexed Fe(II).

Ferrihydrite, a well-crystallized lepidocrocite,[56] the Fh-PGA coprecipitate, and (un)reacted flocs samples were also measured through a range of temperatures (5 to 77 K) in order to determine the blocking temperature; a parameter positively correlated to particle size (SI Figures S8 and S9). Blocking temperature is defined as the temperature at which the summed areas of the doublets and sextets in Mössbauer spectra are equal. In agreement with the literature,[7,28] ferrihydrite and lepidocrocite possessed blocking temperatures between 50 and 77 K (Figure S9). In contrast, the Fh-PGA coprecipitate displayed weak magnetic ordering below 25 K (SI Figure S8) and a blocking temperature of ∼37 K (SI Figure S9); indicating coprecipitation with OM caused a significant decrease in ferrihydrite particle size.[28] Similarly, the unreacted 5S flocs showed weak magnetic ordering below 25 K (SI Figure S8) and exhibited a blocking temperature of ∼32 K (SI Figure S9). Because of the spectral similarities between unreacted 5S and 5L flocs (SI Figure S8) it is assumed floc sample 5L also possessed a similar blocking temperature. Thus, floc Fe particles are of comparative size to the Fh-PGA coprecipitate, and are significantly smaller than the pure Fe(III)-(oxyhydr)-oxides.

Of the Fe(II)-spiked samples, only 5S flocs reacted with 1.0 mM ^{57}Fe(II) at pH 7 was measured at varying temperatures (SI Figure S8) and revealed an increase in the blocking temperature from ∼32 to ∼39 K (SI Figure S9). These changes may reflect a shift in the mineralogical composition (Tables 1 and 2) and/or indicate a larger average mineral particle size after reaction with Fe(II).

Influence of OM on Fe(II)-Catalyzed Fe Atom Exchange and Mineral Transformations. In freshwater wetlands, precipitation of Fe(III)-(oxyhydr)oxides rarely results in pure mineral phases. Rather, naturally occurring Fe minerals are often associated with OM; impeding crystal growth and mineral-transformation reactions. Although this may imply inherently larger mineral surface areas available for Fe(II) adsorption, both the flocs and the Fh-PGA coprecipitate showed reduced Fe atom exchange and mineral transformation as compared to pure ferrihydrite, which, at pH 7, underwent near complete Fe atom exchange and transformed into crystalline Fe(III)-oxyhydroxides within 7 days even at a low $Fe(II)_{spike}$:Fe_{solid} ratio. These results document that carbohydrate-rich OM in flocs effectively impairs the Fe(II)-catalyzed transformation of ferrihydrite, which is consistent with previous studies.[27,28,37]

Reduced Fe atom exchange and Fe(II)-catalyzed mineral transformations caused by floc OM and PGA can have several reasons. First, the adsorption or coprecipitation of OM with Fe(III)-(oxyhydr)oxides could have reduced available sorption sites for Fe(II).[27,57] Chen et al.[57] argued that at C:Fe molar ratios ≥2.8, mineral surface sites and pores of Fh-OM coprecipitates would be completely blocked, thus preventing the initial Fe(II) adsorption step preceding Fe atom exchange and mineral transformations.[15−17] Although *Gola di Lago* flocs have similarly high C:Fe molar ratios (2.2−32.7),[3,4] our recent study on secondary mineralization reactions in the presence of sulfide suggests that complete surface-site blockage may not apply to freshwater flocs: Sulfidization of Fe(III)-(oxyhydr)-oxides proceeds through electron transfer between surface-complexed sulfide and the Fe(III) mineral phase.[58] In our study, sulfidization of floc Fe minerals ($S(-II)_{spike}$:Fe(III) = 0.75−1.62 mol/mol) at pH 7 was rapid (≤0.3 days),[4] indicating that surface sites of the poorly crystalline floc Fe(III)-(oxyhydr)oxides were readily accessible to sulfide (and potentially for Fe(II) as well). Second, Fe(II) could have been preferentially complexed by carboxyl or carboxy-phenolic moieties OM,[59] reducing the extent of Fe(II) adsorption on mineral surfaces and hence inhibiting Fe atom exchange and mineral transformations. This scenario is supported by the appearance of Fe(II) doublets in Mössbauer spectra of Fe(II)-reacted floc and Fh-PGA samples (Table 2). In fact, the Fe(II) doublets accounted for 29−190% ($\bar{x}$ = 140%) of total Fe(II) added. Discrepancies in the Fe(II) mass balance may be attributed to large errors in the small Fe(II) abundances calculated from Mössbauer spectra fits. Finally, adsorption of Fe(II) onto Fe(III)-(oxyhydr)oxide surfaces could have resulted in a labile Fe surface layer[17,44,60] which may include ferrous and ferric Fe.[44] Iron in this ^{57}Fe-enriched reactive layer could have desorbed as ^{57}Fe(II)[44] or, in the presence of organic ligands, as ^{57}Fe(II/III)-OM complexes,[61] thus reducing the net

DOI: 10.1021/acs.est.7b01495
Environ. Sci. Technol. 2017, 51, 6897−6907

Fe atom exchange. The existence of a labile Fe surface layer vulnerable to ligand-promoted dissolution would also explain increases in Fe_{aq} detected for the OM-containing samples (Figure 1 and SI Figure S2). This notion is supported by the lack of Fe_{aq} increases in the controls, where no reactive surface layer could have formed in the absence of Fe(II).

Environmental Implications. The results of this study imply that, in environmental systems where solid-solution equilibria are rapidly attained, carbohydrate-rich OM stabilizes poorly crystalline Fe(III)-(oxyhydr)oxide minerals against Fe(II)-catalyzed reductive transformation at circumneutral pH, which potentially lowers the extent of trace metal(loid) release. Our findings indicate that the results of similar abiotic experiments using pure Fe(III)-(oxyhydr)oxides showing a pronounced effect of Fe(II)-activated trace metal(loid) release and redistribution[31,35,62] may not be transferable to organic-rich freshwater floc environments, where Fe atom exchange and mineral transformations are impaired due to partial surface-site blockage by sorbed OM and/or organic Fe(II) complexation. The latter implies that the capacity of floc OM to bind aqueous Fe(II) exerts an additional important abiotic control on the Fe(II)-activated trace element release from freshwater flocs.

Freshwater wetlands often undergo frequent and rapid changes in the redox potential resulting from fluctuating water tables and shifts in microbial activity.[63] For freshwater flocs existing in such redox-dynamic environments, the results of this study indicate that short-term (≤7 days) exposure of flocs to Fe(II) pulses does not affect their ability to retain trace metal(loid)s. Under these conditions, freshwater flocs may still be considered important sinks for trace elements.

■ ASSOCIATED CONTENT

Supporting Information

The Supporting Information is available free of charge on the ACS Publications website at DOI: 10.1021/acs.est.7b01495.

Details on floc sampling location, experimental conditions, total element contents, calculations and tables of isotope data and isotope mass balance, and additional solid-phase Fe speciation data (PDF)

■ AUTHOR INFORMATION

Corresponding Author

*E-mail: christian.mikutta@env.ethz.ch.

ORCID

Christian Mikutta: 0000-0002-4363-0972
Andreas Kappler: 0000-0002-3558-9500
Ruben Kretzschmar: 0000-0003-2587-2430

Notes

The authors declare no competing financial interest.

■ ACKNOWLEDGMENTS

We are grateful to K. Barmettler (ETH Zurich) for assisting with laboratory analyses. We acknowledge APS, a User Facility of the U.S. Department of Energy Office of Science operated by Argonne National Laboratory, contract No. DE-AC02-06CH11357 for the provision of synchrotron radiation facilities and thank Q. Ma for support during the synchrotron measurements. This project was funded by the SNSF (Project 200021_127157).

■ REFERENCES

(1) Elliott, A. V. C.; Plach, J. M.; Droppo, I. G.; Warren, L. A. Comparative floc-bed sediment trace element partitioning across variably contaminated aquatic ecosystems. *Environ. Sci. Technol.* **2012**, *46*, 209−216.

(2) Plach, J. M.; Elliott, A. V. C.; Droppo, I. G.; Warren, L. A. Physical and ecological controls on freshwater floc trace metal dynamics. *Environ. Sci. Technol.* **2011**, *45*, 2157−2164.

(3) ThomasArrigo, L. K.; Mikutta, C.; Byrne, J.; Barmettler, K.; Kappler, A.; Kretzschmar, R. Iron and arsenic speciation and distribution in organic flocs from streambeds of an arsenic-enriched peatland. *Environ. Sci. Technol.* **2014**, *48*, 13218−13228.

(4) ThomasArrigo, L. K.; Mikutta, C.; Lohmayer, R.; Planer-Friedrich, B.; Kretzschmar, R. Sulfidization of organic freshwater flocs from a minerotrophic peatland: Speciation changes of iron, sulfur, and arsenic. *Environ. Sci. Technol.* **2016**, *50*, 3607−3616.

(5) Elliott, A. V. C.; Warren, L. A. Microbial engineering of floc Fe and trace metal geochemistry in a circumneutral, remote lake. *Environ. Sci. Technol.* **2014**, *48*, 6578−6587.

(6) Schwertmann, U.; Taylor, R. M. Natural and synthetic poorly crystallized lepidocrocite. *Clay Miner.* **1979**, *14*, 285−293.

(7) Cornell, R. M.; Schwertmann, U. *The Iron Oxides: Structure, Properties, Reactions, Occurances and Uses*; Wiley-VCH: Weinheim, Germany, 2003.

(8) Posth, N. R.; Huelin, S.; Konhauser, K. O.; Kappler, A. Size, density and composition of cell-mineral aggregates formed during anoxygenic phototrophic Fe(II) oxidation: Impact on modern and ancient environments. *Geochim. Cosmochim. Acta* **2010**, *74*, 3476−3493.

(9) Ploug, H.; Kühl, M.; Buchholz-Cleven, B.; Jørgensen, B. B. Anoxic aggregates - an ephemeral phenomenon in the pelagic environment? *Aquat. Microb. Ecol.* **1997**, *13*, 285−294.

(10) Elliott, A. V. C.; Plach, J. M.; Droppo, I. G.; Warren, L. A. Collaborative microbial Fe-redox cycling by pelagic floc bacteria across wide ranging oxygenated aquatic systems. *Chem. Geol.* **2014**, *366*, 90−102.

(11) Droppo, I. G.; Leppard, G. G.; Flannigan, D. T.; Liss, S. N. The freshwater floc: A functional relationship of water and organic and inorganic floc constituents affecting suspended sediment properties. *Water, Air, Soil Pollut.* **1997**, *99*, 43−53.

(12) Liss, S. N.; Droppo, I. G.; Flannigan, D. T.; Leppard, G. G. Floc architecture in wastewater and natural riverine systems. *Environ. Sci. Technol.* **1996**, *30*, 680−686.

(13) Balzano, S.; Statham, P. J.; Pancost, R. D.; Lloyd, J. R. Role of microbial populations in the release of reduced iron to the water column from marine aggregates. *Aquat. Microb. Ecol.* **2009**, *54*, 291−303.

(14) Lu, S.; Chourey, K.; Reiche, M.; Nietzsche, S.; Shah, M. B.; Neu, T. R.; Hettich, R. L.; Küsel, K. Insights into the structure and metabolic function of microbes that shape pelagic iron-rich aggregates ("Iron Snow"). *Appl. Environ. Microb.* **2013**, *79*, 4272−4281.

(15) Handler, R. M.; Beard, B. L.; Johnson, C. M.; Scherer, M. M. Atom exchange between aqueous Fe(II) and goethite: An Fe isotope tracer study. *Environ. Sci. Technol.* **2009**, *43*, 1102−1107.

(16) Handler, R. M.; Frierdich, A. J.; Johnson, C. M.; Rosso, K. M.; Beard, B. L.; Wang, C.; Latta, D. E.; Neumann, A.; Pasakarnis, T.; Premaratne, W. A. P. J.; Scherer, M. M. Fe(II)-catalyzed recrystallization of goethite revisited. *Environ. Sci. Technol.* **2014**, *48*, 11302−11311.

(17) Boland, D.; Collins, R.; Miller, C.; Glover, C.; Waite, T. D. Effect of solution and solid-phase conditions on the Fe(II)-accelerated transformation of ferrihydrite to lepidocrocite and goethite. *Environ. Sci. Technol.* **2014**, *48*, 5477−5485.

(18) Mikutta, C.; Wiederhold, J. G.; Cirpka, O. A.; Hofstetter, T. B.; Bourdon, B.; Von Gunten, U. Iron isotope fractionation and atom exchange during sorption of ferrous iron to mineral surfaces. *Geochim. Cosmochim. Acta* **2009**, *73*, 1795−1812.

DOI: 10.1021/acs.est.7b01495
Environ. Sci. Technol. 2017, 51, 6897−6907

(19) Frierdich, A. J.; Helgeson, M.; Liu, C.; Wang, C.; Rosso, K. M.; Scherer, M. M. Iron atom exchange between hematite and aqueous Fe(II). *Environ. Sci. Technol.* **2015**, *49*, 8479−8486.
(20) Hansel, C. M.; Benner, S. G.; Fendorf, S. Competing Fe(II)-induced mineralization pathways of ferrihydrite. *Environ. Sci. Technol.* **2005**, *39*, 7147−7153.
(21) Pedersen, H. D.; Postma, D.; Jakobsen, R.; Larsen, O. Fast transformation of iron oxyhydroxides by the catalytic action of aqueous Fe(II). *Geochim. Cosmochim. Acta* **2005**, *69*, 3967−3977.
(22) Yang, L.; Steefel, C.; Marcus, M. A.; Bargar, J. R. Kinetics of Fe(II)-catalyzed transformation of 6-line ferrihydrite under anaerobic flow conditions. *Environ. Sci. Technol.* **2010**, *44*, 5469−5475.
(23) Pedersen, H. D.; Postma, D.; Jakobsen, R. Release of arsenic associated with the reduction and transformation of iron oxides. *Geochim. Cosmochim. Acta* **2006**, *70*, 4116−4129.
(24) Ford, R. G. Rates of hydrous ferric oxide crystallization and the influence on coprecipitated arsenate. *Environ. Sci. Technol.* **2002**, *36*, 2459−2463.
(25) Gomez, M. A.; Hendry, M. J.; Hossain, A.; Das, S.; Elouatik, S. Abiotic reduction of 2-line ferrihydrite: effects on adsorbed arsenate, molybdate, and nickel. *RSC Adv.* **2013**, *3*, 25812−25822.
(26) Hansel, C. M.; Learman, D. R.; Lentini, C. J.; Ekstrom, E. B. Effect of adsorbed and substituted Al on Fe(II)-induced mineralization pathways of ferrihydrite. *Geochim. Cosmochim. Acta* **2011**, *75*, 4653−4666.
(27) Jones, A. M.; Collins, R. N.; Rose, J.; Waite, T. D. The effect of silica and natural organic matter on the Fe(II)-catalysed transformation and reactivity of Fe(III) minerals. *Geochim. Cosmochim. Acta* **2009**, *73*, 4409−4422.
(28) Chen, C.; Kukkadapu, R. K.; Sparks, D. L. Influence of coprecipitated organic matter on $Fe^{2+}_{(aq)}$-catalyzed transformation of ferrihydrite: Implications for carbon dynamics. *Environ. Sci. Technol.* **2015**, *49*, 10927−10936.
(29) Muehe, E. M.; Scheer, L.; Daus, B.; Kappler, A. Fate of arsenic during microbial reduction of biogenic versus abiogenic As-Fe(III)-mineral coprecipitates. *Environ. Sci. Technol.* **2013**, *47*, 8297−8307.
(30) Cummings, D. E.; Caccavo, F.; Fendorf, S.; Rosenzweig, R. F. Arsenic mobilization by the dissimilatory Fe(III)-reducing bacterium *Shewanella alga* BrY. *Environ. Sci. Technol.* **1999**, *33*, 723−729.
(31) Frierdich, A. J.; Catalano, J. G. Controls on Fe(II)-activated trace element release from goethite and hematite. *Environ. Sci. Technol.* **2012**, *46*, 1519−1526.
(32) Jang, J. H.; Dempsey, B. A.; Catchen, G. L.; Burgos, W. D. Effects of Zn(II), Cu(II), Mn(II), Fe(II), NO_3^-, or SO_4^{2-} at pH 6.5 and 8.5 on transformations of hydrous ferric oxide (HFO) as evidenced by Mössbauer spectroscopy. *Colloids Surf., A* **2003**, *221*, 55−68.
(33) Coughlin, B. R.; Stone, A. T. Nonreversible adsorption of divalent metal-ions (Mn^{II}, Co^{II}, Ni^{II}, Cu^{II}, and Pb^{II}) onto goethite: Effects of acidification, Fe^{II} addition, and picolinic acid addition. *Environ. Sci. Technol.* **1995**, *29*, 2445−2455.
(34) Nico, P. S.; Stewart, B. D.; Fendorf, S. Incorporation of oxidized uranium into Fe (hydr)oxides during Fe(II) catalyzed remineralization. *Environ. Sci. Technol.* **2009**, *43*, 7391−7396.
(35) Frierdich, A. J.; Catalano, J. G. Fe(II)-mediated reduction and repartitioning of structurally incorporated Cu, Co, and Mn in iron oxides. *Environ. Sci. Technol.* **2012**, *46*, 11070−11077.
(36) Mikutta, C.; Mikutta, R.; Bonneville, S.; Wagner, F.; Voegelin, A.; Christl, I.; Kretzschmar, R. Synthetic coprecipitates of exopolysaccharides and ferrihydrite. Part 1: Characterization. *Geochim. Cosmochim. Acta* **2008**, *72*, 1111−1127.
(37) Henneberry, Y. K.; Kraus, T. E. C.; Nico, P. S.; Horwath, W. R. Structural stability of coprecipitated natural organic matter and ferric iron under reducing conditions. *Org. Geochem.* **2012**, *48*, 81−89.
(38) Schwertmann, U.; Cornell, R. M. *Iron Oxides in the Laboratory: Preparation and Characterization*; WILEY-VCH Verlag GMBH & Co. KGaA: Weinheim, Germany, 2000.
(39) Hofmann, A.; Pelletier, M.; Michot, L.; Stradner, A.; Schurtenberger, P.; Kretzschmar, R. Characterization of the pores in hydrous ferric oxide aggregates formed by freezing and thawing. *J. Colloid Interface Sci.* **2004**, *271*, 163−173.
(40) Taylor, P. D. P.; Maeck, R.; Debievre, P. Determination of the absolute isotopic composition and atomic weight of a reference sample of natural iron. *Int. J. Mass Spectrom. Ion Processes* **1992**, *121*, 111−125.
(41) Koretsky, C. M.; Haveman, M.; Beuving, L.; Cuellar, A.; Shattuck, T.; Wagner, M. Spatial variation of redox and trace metal geochemistry in a minerotrophic fen. *Biogeochemistry* **2007**, *86*, 33−62.
(42) Boulegue, J.; Lord, C. J.; Church, T. M. Sulfur speciation and associated trace-metals (Fe, Cu) in the pore waters of Great Marsh, Deleware. *Geochim. Cosmochim. Acta* **1982**, *46*, 453−464.
(43) Mikutta, C.; Kretzschmar, R. Synthetic coprecipitates of exopolysaccharides and ferrihydrite. Part II: Siderophore-promoted dissolution. *Geochim. Cosmochim. Acta* **2008**, *72*, 1128−1142.
(44) Tishchenko, V.; Meile, C.; Scherer, M. M.; Pasakarnis, T. S.; Thompson, A. Fe^{2+} catalyzed iron atom exchange and re-crystallization in a tropical soil. *Geochim. Cosmochim. Acta* **2015**, *148*, 191−202.
(45) Wu, L.; Beard, B. L.; Roden, E. E.; Johnson, C. M. Stable iron isotope fractionation between aqueous Fe(II) and hydrous ferric oxide. *Environ. Sci. Technol.* **2011**, *45*, 1847−1852.
(46) Ravel, B.; Newville, M. ATHENA, ARTEMIS, HEPHAESTUS: data analysis for X-ray absorption spectroscopy using IFEFFIT. *J. Synchrotron Radiat.* **2005**, *12*, 537−541.
(47) Lagarec, K.; Rancourt, D. G. Extended Voigt-based analytic lineshape method for determining N-dimensional correlated hyperfine parameter distributions in Mossbauer spectroscopy. *Nucl. Instrum. Methods Phys. Res., Sect. B* **1997**, *129*, 266−280.
(48) Williams, A. G. B.; Scherer, M. M. Spectroscopic evidence for Fe(II)-Fe(III) electron transfer at the iron oxide-water interface. *Environ. Sci. Technol.* **2004**, *38*, 4782−4790.
(49) Tomaszewski, E. J.; Cronk, S. S.; Gorski, C. A.; Ginder-Vogel, M. The role of dissolved Fe(II) concentration in the mineralogical evolution of Fe (hydr)oxides during redox cycling. *Chem. Geol.* **2016**, *438*, 163−170.
(50) Reddy, T. R.; Frierdich, A. J.; Beard, B. L.; Johnson, C. M. The effect of pH on stable iron isotope exchange and fractionation between aqueous Fe(II) and goethite. *Chem. Geol.* **2015**, *397*, 118−127.
(51) Eusterhues, K.; Wagner, F. E.; Häusler, W.; Hanzlik, M.; Knicker, H.; Totsche, K. U.; Kögel-Knabner, I.; Schwertmann, U. Characterization of ferrihydrite-soil organic matter coprecipitates by X-ray diffraction and Mössbauer spectroscopy. *Environ. Sci. Technol.* **2008**, *42*, 7891−7897.
(52) Murad, E. The Mössbauer spectrum of 'well'-crystallized ferrihydrite. *J. Magn. Magn. Mater.* **1988**, *74*, 153−157.
(53) Murad, E.; Schwertmann, U. The influence of crystallinity on the Mössbauer spectrum of lepidocrocite. *Mineral. Mag.* **1984**, *48*, 507−511.
(54) Dyar, M. D.; Agresti, D. G.; Schaefer, M. W.; Grant, C. A.; Sklute, E. C. Mössbauer spectroscopy of earth and planetary materials. *Annu. Rev. Earth Planet. Sci.* **2006**, *34*, 83−125.
(55) Génin, J. M. R.; Bourrie, G.; Trolard, F.; Abdelmoula, M.; Jaffrezic, A.; Refait, P.; Maitre, V.; Humbert, B.; Herbillon, A. Thermodynamic equilibria in aqueous suspensions of synthetic and natural Fe(II)-Fe(III) green rusts: Occurrences of the mineral in hydromorphic soils. *Environ. Sci. Technol.* **1998**, *32*, 1058−1068.
(56) Borer, P.; Sulzberger, B.; Hug, S. J.; Kraemer, S. M.; Kretzschmar, R. Photoreductive dissolution of iron(III) (hydr)oxides in the absence and presence of organic ligands: Experimental studies and kinetic modeling. *Environ. Sci. Technol.* **2009**, *43*, 1864−1870.
(57) Chen, C. M.; Dynes, J. J.; Wang, J.; Sparks, D. L. Properties of Fe-organic matter associations via coprecipitation versus adsorption. *Environ. Sci. Technol.* **2014**, *48*, 13751−13759.
(58) Poulton, S. W.; Krom, M. D.; Raiswell, R. A revised scheme for the reactivity of iron (oxyhydr)oxide minerals towards dissolved sulfide. *Geochim. Cosmochim. Acta* **2004**, *68*, 3703−3715.
(59) Catrouillet, C.; Davranche, M.; Dia, A.; Bouhnik-Le Coz, M.; Marsac, R.; Pourret, O.; Gruau, G. Geochemical modeling of Fe(II) binding to humic and fulvic acids. *Chem. Geol.* **2014**, *372*, 109−118.

DOI: 10.1021/acs.est.7b01495
Environ. Sci. Technol. 2017, 51, 6897−6907

(60) Amstaetter, K.; Borch, T.; Larese-Casanova, P.; Kappler, A. Redox transformation of Arsenic by Fe(II)-activated goethite (α-FeOOH). *Environ. Sci. Technol.* **2010**, *44*, 102−108.
(61) Royer, R. A.; Burgos, W. D.; Fisher, A. S.; Unz, R. F.; Dempsey, B. A. Enhancement of biological reduction of hematite by electron shuttling and Fe(II) complexation. *Environ. Sci. Technol.* **2002**, *36*, 1939−1946.
(62) Frierdich, A. J.; Luo, Y.; Catalano, J. G. Trace element cycling through iron oxide minerals during redox-driven dynamic recrystallization. *Geology* **2011**, *39*, 1083−1086.
(63) Reddy, K. R.; DeLaune, R. D. *Biogeochemistry of wetlands: Science and applications*; CRC Press: Boca Raton, 2008.
(64) Kelly, S. D.; Hesterberg, D.; Ravel, B., Analysis of soils and minerals using X-ray absorption spectroscopy. In *Methods of Soil Analysis. Part 5. Minerological Methods*; Ulery, A. L.; Drees, L. R., Eds.; Soil Science Society of America: Madison, 2008; pp 378−463.

DOI: 10.1021/acs.est.7b01495
Environ. Sci. Technol. 2017, 51, 6897−6907